Efficiency-Oriented Design of Litz Wire for Several kW Power Experimented on 20 kW Prototype

Damien Lemaitre, Benoît Sarrazin, Yohan Wanderoild, Yves Lembeye, Alexis Derbey

Efficiency-Oriented Design of Litz Wire for Several kW Power Experimented on 20 kW Prototype.

Damien LEMAITRE[1,2], Benoît SARRAZIN[2], Yohan WANDEROILD[1], Yves LEMBEYE[2], Alexis Derbey[2]

[1]EDF R&D, EDF Lab Les Renardières, département TREE, 77250 Moret-Loing et Orvanne, France
[2]Univ. Grenoble Alpes, CNRS, Grenoble INP, G2Elab 38000 Grenoble, France

Corresponding author: Damien Lemaitre, damien.lemaitre@grenoble-inp.fr

Abstract

Wireless Power Transfer (WPT) from a few kW to hundreds of kW is the future in order to simplify the recharging of electric vehicles (EVs). For ensuring high current ratings in the magnetic couplers used for this transfer, Litz wire conductors are used to deal with the skin effect due to the 85 kHz operating frequency imposed by SAE standards. These conductors are made by paralleling a more or less large number of strands of Litz wires. Depending on the Litz wire design, inhomogeneous current distributions between these strands can be observed. This article highlights this phenomenon by real measurements carried out on two 20 kW WPT prototypes and study the relevant parameters to propose solutions. Tests on different designs, different connectors at the ends, as well as an easy way to perform Litz wire test method are provided. Finally, the proposals developed and validated experimentally made it possible to obtain a new prototype with a 20% reduction in winding losses while dividing the necessary quantity of copper volume by 2.5.

1 Introduction

1.1 Context

Wireless power transfer system (WPTS) for EV charging has great potential in V2G application thanks to its very easy connection with network. The use of these devices is also envisaged in the development of autonomous EVs because they make it possible to avoid human intervention in the recharging phase. Fig 1 and Fig 2 show respectively a picture of the principle of static WPTS and the electrical schematic that can be used in a series-series resonant compensation (SS) converter for WPTS.

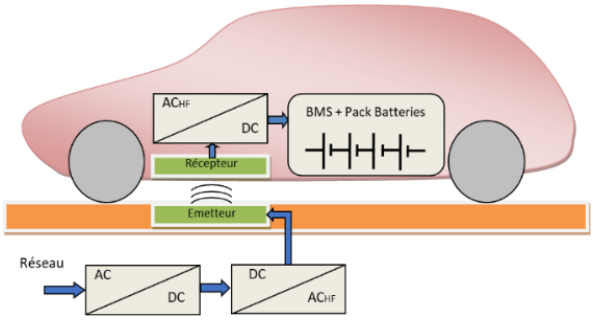

Fig 1: WPT principle of an EV static charging

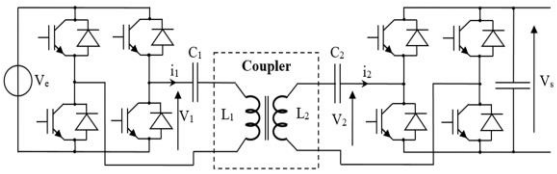

Fig 2: Schematic of a series-series resonant DC-DC converter

SS topology has very interesting characteristics for WPTS thanks to the independence from load and magnetic coupling of primary capacitors [1]–[6]. Performances reached at high power make SS topology suitable for several kW WPTS [5], [7]. Combination of resonant compensation capacitor, high efficient converter [8]–[10], zero voltage switching (ZVS) made possible to reach very high efficiency.

It has been proved thanks to prototypes in [11]–[14] with following output power and efficiency between DC bus: [5 kW; 96.5%], [10.4 kW; 94.4%], [20 kW; 95.0%], and [20 kW; 95.5%] respectively. Losses analysis of the introduced prototypes shows important losses in windings and converters.

The latter are performing better year after year thanks to ever more efficient switches. Improvements in the method for reducing winding losses are, however, necessary due to complexity of the phenomena involved in Litz wire (LW) losses.

Improving winding efficiency is therefore one of the biggest challenges in WPTS [15].

1.2 Previous work

Previous work [14] shows that 51% of the total losses in the WPT prototype come from windings as described on Fig 3. Windings are made with LW that are widely used in WPTS, as [11]–[14], to reduce skin effect (SE) losses. This first prototype uses LW n°1, presented in Table 1.

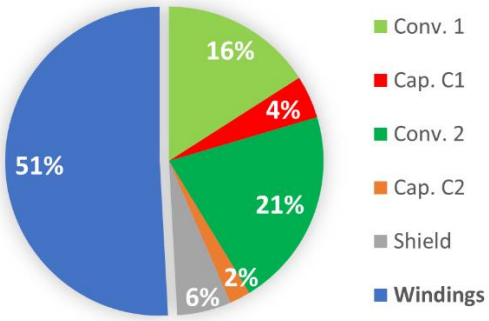

Fig 3: Losses distribution of 20 kW WPT prototype n°1, using LW n°1 at 81 kHz, with 96.2% efficiency between DC to DC.

The loss distribution in Fig 3 is obtained by measuring the input and output powers. Subtracting the total losses from the calculated losses in the converters and capacitors gives coupler losses. The losses in the ferrite and aluminium shielding are then calculated by a finite element method (FEM) to obtain the losses in the Litz wires.

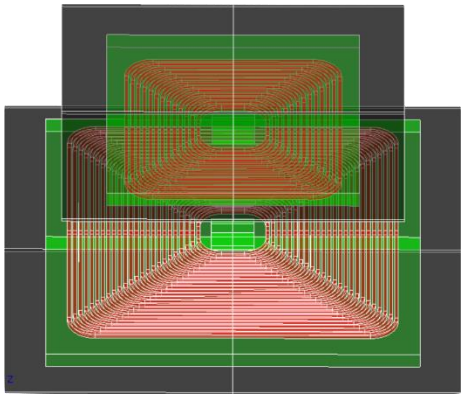

Fig 4: 3D Simulation of 20 kW prototype 1

Simulated ferrite losses are calculated using Steinmetz equation and are evaluated at 3.5 W. This result is consistent due to the large ferrite thickness of 28 mm, which significantly reduces the amplitude of the induction in the ferrite. In addition, ferrite losses are almost cubically proportional to the induction level.

Shield losses for primary and secondary are evaluated at 45 W. The analyses of the current distribution in a LW guided the choice of an adapted LW which permitted to reduce the winding losses by 20% while reducing copper volume and cost by a factor 2.5 and 3.4 respectively, as validated below in part 3.3.

2 Litz design

2.1 Construction

LW design aims to reduce skin effect (SE) losses by using a stranded wire with individually insulated conductors to constitute a bundle. The bundles can then be joined together to form another bigger one of a higher level, see Fig 5.

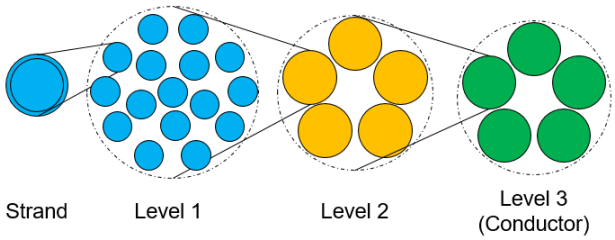

Fig 5: Example of a LW design that consists of five bundles, each consisting of five sub-bundles, each consisting of 16 strands: 5x5x16 (Lvl3 x Lvl2 x Lvl1).

Strands and bundles interactions generate proximity effects resulting in extra losses due to heterogeneous induced current distribution.

Many parameters are involved in LW design, which are:

- Strand, Bundle and LW copper cross section diameter
- Number of strands/bundles per level
- Number of levels
- Pitch length and direction (S or Z)
- LW fil factor and shape (round, square...)
- braided or twisted LW
- Twist/braid imperfection

All of these parameters influence price and efficiency of the LW. The results on the LW 1 used on prototype 1 show a very heterogeneous current distribution, described in Table 1.

Comparing with the ideal case of a homogeneous current distribution, the additional DC losses generated are higher than 50%. A design to improve power distribution is therefore a priority in order to reduce losses in the windings.

2.2 Improvements

Current distribution is related to the LW design as presented in [16]–[18] and because the current in the centre bundle I_c could be phase shifted compared to current in peripheral bundles I_p. This phase shift depends on the frequency as it is shown in [16] and becomes higher than 150° at the frequencies above 80 kHz. It is therefore recommended to limit bundle number per level to a maximum of five as illustrated on Fig 6 (b). If not, a heterogeneous current distribution due to the presence of a central bundle as shown in Fig 6 (a) is obtained. The tests carried out on LW n°1, n°2 and n°3 presented in Table 2 have confirmed the importance of this rule for currents of around ten amperes.

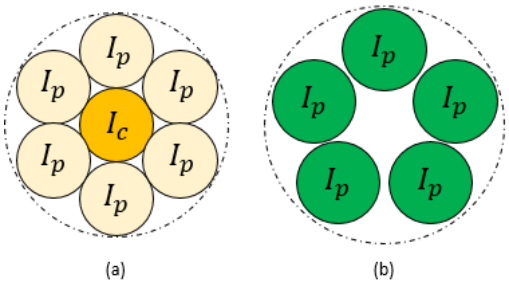

Fig 6: (a) Litz wire design breaking bundles position rule, introducing phase shift current Ic. (b) Litz wire design respecting bundles position

	LW n°1	LW n°2	LW n°3
Copper section	25 mm2	10 mm2	10.2 mm2
LW section	53.9 mm2	19.4 mm2	20.3 mm2
Strands number	3184*	1275	1296
Strand Diameter	0.1 mm	0.1 mm	0.1 mm
Bundles number			
Level 1	16	5	6
Level 2	10	5	6
Level 3	20*	51	6
Level 4	/	/	6

Table 1: *Characteristics of LW design tested, LW n°1 (16x10x20), LW n°2 (5x5x51) and LW n°3 (6x6x6x6). * One of the 10 bundles of level 2 of the LW n°2 has 19 strands instead of 20.*

The connectors of LW also seem to have an influence on the current distribution [19], [20].

An experimental test illustrated in Fig 9 is carried out to study changes made by dividing the connectors. Following part presents the sizing method used to design prototypes.

3 Experimentations on Litz Wire

In this part, tests protocol and results are described. Influence of two connectors, LW design, and LW test method are evaluated.

WPTS 20 kW output power system used to make experimentations is described in [14] and presented on Fig 7. Primary and secondary windings number of turns, and outer diameters, are N1 = 24 and N2 = 13, Dout1 = 560 mm and Dout2 = 360 mm. Both windings have the same inner diameter of Din = 50 mm. Air gap between windings is E = 21 cm. Resonant capacitors C1 and C2 used for primary and secondary compensation are Celem CSM 150/200 with capacitance value and withstand voltage per unit of 100 nF and 1,000 V. Their values are 12.5 nF and 50 nF respectively.

Fig 7: Overall experimental setup

Many simulated results and experimentations at low currents to analyse the influence of LW design are present in the literature but no comparison of LW design on WPTS of several tens of kW showing the influence of this design were found. It is the reason why we have focused on this point and following results in order to show the importance of rules on bundles number for high power WPTS and to propose guidelines for their improvements.

3.1 Demonstrators

The two demonstrators on Fig 8 have been tested to achieve this goal. Windings of the first one Fig 8 (a) and of the second one Fig 8 (b) are realized with LW n°1 and LW n°2 respectively. Table 1 presents characteristics of LW used.

The two tested WPTS are similar from DC to DC at the exception of LW to have a conclusive comparison. It means the same converters, the same command and the same capacitors are used. Couplers of the two prototypes have the same N1, N2, E, Din, Dout, shielding and ferrite dimensions. Only inter-coils space is changing to obtain the same inner and outer winding diameters due to the different LW diameters.

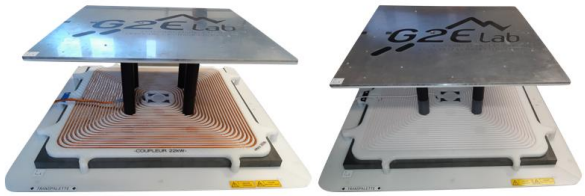

Fig 8: Prototype n°1 with LW n°1 (a) and prototype n°2 with LW n°2 (b) to constitute windings of the coupler.

Measuring tools used for following measures are the current probes. The latter are connected to LeCroy waverunner HRO 66ZIis for display and data processing.

3.2 Tests on connectors influences

3.2.1 Theory

A first test to improve current distribution in the LW n°1 consists in dividing terminal at LW ending by two terminals to increase the number of peripheral bundles as represented in Fig 9. In fact, the connectors could have no negligible impact on current distribution due to the melting process to link connectors and LW [19], [20].

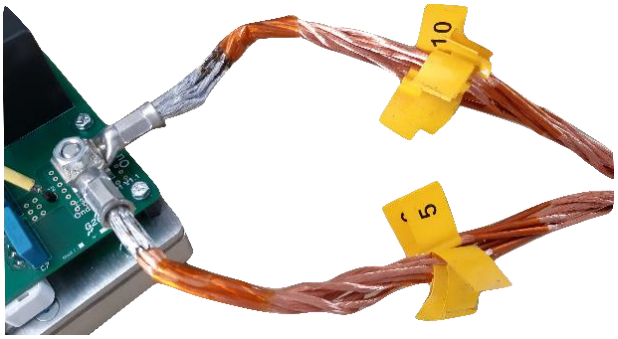

Fig 9: LW n°1 with two connectors at each end. The 16 bundles of the level n°1 are divided in two groups of 8 connectors.

Bundles at level 3 of LW n°1 used for this test (characteristics Table 1) are divided in two groups of eight bundles, each with its own connector. It enables to have only two centre bundles instead of three in the case of one connector for the 16 bundles of LW n°1. Skin effect described in [20] at the connectors is thus supposed to be reduced.

3.2.2 Results

The observed current distribution is the same in each LW bundle whether using one or two connectors per termination. This results differ from those of [19], [20] and could find explanations in the different soldering process. The recommended one in [21] has been followed to realize the presented LW connections. Steps of method followed here consist of immersing the Litz wire in a tin bath at 400°C for a duration depending on the LW cross section. The tin plating must be carried out over a length greater than the last level bundle pitch, see Fig *5*. Similar process is recommended in [22]. The way used in [19], [20] to solder the connectors seem to be different. In fact, it seems that the method used leaves the insulation on the outside of the LW. However, this is not the case by immersing the wire in the soldering pot as described by LW manufacturers in [21], [22].

Obtaining the same current in each bundle for the two cases studied shows that the influence of the LW design is more important than the influence of the connectors.

3.3 Litz Wire design tests

In this section, the current distributions obtained in the three LW, shown in Table 2 are compared.

3.3.1 Comparison Method

A simple and efficient method for measuring the power distribution of a LW has been implemented. A small length is required for this test avoiding the need of a coupler to observe the current distribution in the LW. Influences on the current distribution between primary and secondary and between windings can be neglected due to the influence of the LW design. The assumption was made that the influence of design is dominant over the inter-spiral influence on current distribution. This method has been experimentally validated with prototypes n°1 and n°2. The protocol followed to validate this method consists in measuring current distribution in LW n°1 constituting the primary winding of prototype n°1. Then a comparison is made with current distribution in a sample of the same LW connected between the inverter and the resonant converter. By this way, both parts of tested LW have the same current flowing

through them and they do not have any influence on each other.

The LW sample length is 10 times greater than the bundle pitch of the tested LW to ensure that each bundle sees the same field on average.

LW sample is hung up in the air as shown in the Fig 11 to ensure that there are no source of interference near the LW. Exactly the same current distribution was found in the sample and in the LW constituting the primary of the coupler.

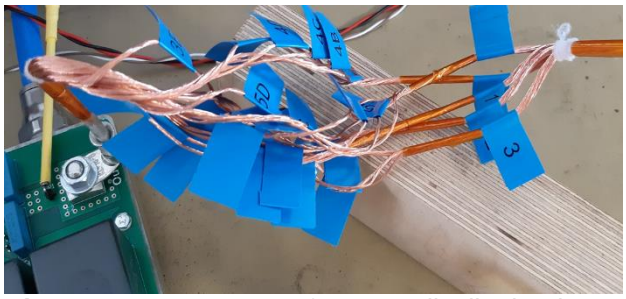

Fig 10: *Measurements of current distribution in LW n°2 sample.*

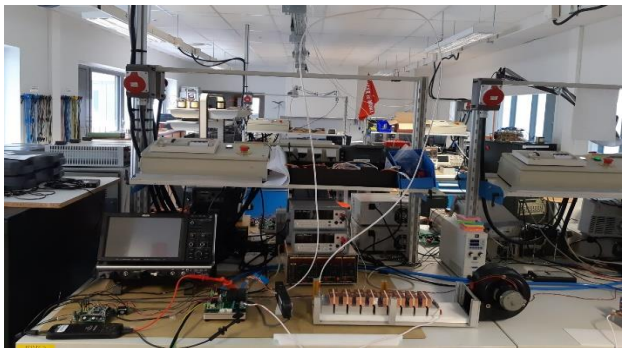

Fig 11: Measurements of current distribution in LW n°2 on the three metres long sample

3.3.2 Current distribution

Current distribution has been measured in LW n°1, n°2 and n°3 with the method presented previously. Results are given in Table 2. Measured currents in the 16 bundles at the first level LW n°1 are very heterogeneous. Phase shifts higher than 150° are observed in bundles n°9, n°10, and n°14 compared to the Litz wire current phase, as shown in Table 2.

The phase shift observed for bundles n°6 of LW n°3, however, shows a phase shift of 78° with the total current flowing through the LW. This difference with the expected phase shift is explained by the fact that bundle n°6 is partially in the centre of the LW. Indeed, LW n°3 has a rectangular structure and bundle n° 6 has a part exposed to the external magnetic field.

Litz wire n°1

$P_{out} = 5\ kW,\ \ f = 82.47\ kHz,\ \ I_{LW} = 27.5\ A_{rms}$

Bundle	I_{eff} (A)	$P_{DC}\ (W)$	$E_{rr}\ I_{eff}$ (%)	Phase shift
1	4.08	6.7	137	No
2	2.76	3.0	60	No
3	3.41	4.6	98	No
4	1.34	0.7	22	No
5	2.83	3.2	64	No
6	1.34	0.7	22	No
7	3.46	4.8	101	No
8	3.04	3.7	77	No
9	1.48	0.9	186	162°
10	1.27	0.6	174	178°
11	3.61	5.2	110	No
12	2.12	1.8	23	No
13	1.98	1.6	15	No
14	1.91	15	211	165°
15	0.61	0.1	65	No
16	1.63	1.1	6	No
Sum	36.87	40.2		Phase shift

Litz wire n°2

$P_{out} = 5\ kW,\ \ f = 81.99\ kHz,\ \ I_{LW} = 27.0\ A_{rms}$

Bundle	I_{eff} (A)	$P_{DC}\ (W)$	$E_{rr}\ I_{eff}$ (%)	Phase shift
1	4.77	6.8	8	No
2	6.19	11.5	20	No
3	4.77	6.8	8	No
4	5.48	9.0	6	No
5	5.80	10.1	12	No
Sum	27.01	44.2		In Phase

Litz wire n°3

$P_{out} = 5\ kW,\ \ f = 81.04\ kHz,\ \ I_{LW} = 28.5\ A_{rms}$

Bundle	I_{eff} (A)	$P_{DC}\ (W)$	$E_{rr}\ I_{eff}$ (%)	Phase shift
1	5.2	7.2	9	No
2	6.7	11.9	41	No
3	6.7	11.9	41	No
4	4.8	6.1	1	No
5	4.3	4.9	9	No
6	0.8	0.2	83	78
Sum	28.5	42.2		Phase shift

Table 2: Measured of bundles currents in LW n°1, LW n°2 and LW n°3 for the described output power P_{out}, frequency f and LW total current I_{LW}.

The results obtained with LW n°2 show that these current shifts are avoided by limiting the number of bundles to a maximum of five. In addition, the relative error between the current value measured in each bundles and their average value is much better, even for bundles that do not show a phase shift with the total current. These three tests show the great heterogeneity of the current distribution in the LW when the five-bundles limit is exceeded. The average relative error of the bundles currents for LW n°1, n°2, n°3 are respectively 86%, 11% and 47%.

However, limitations may appear in the design of the LW and especially in WPTS where strong currents flow at high frequencies. At a fixed current density, an increase in current implies an increase in copper surface area. However, the frequency fixes the strand diameter. Knowing the skin depth δ, the latter is recommended to be less than 0.7δ in [23]–[25], less than 2δ in [26], or calculated according equations given in [17], [27]. An increase in copper surface area therefore implies an increase in the number of strands. For a good current distribution, the number of strands per strand is limited to $n_{1,Max}$ given in [17].

We see that the recommendations may be difficult to meet for high power WPTS while avoiding high current density. However, previous and subsequent tests show that it is preferable to reduce the copper surface area in order to achieve compliance with these design rules. The current density will be higher, but will still provide better efficiency. In addition, significant cost savings can be made.

3.4 Prototypes comparisons

Fig 12 shows the efficiency curves as a function of output power for prototypes 1 and 2. Prototype n°2 shows a better DC to DC efficiency at 20 kW of 96.5% instead of 96.2% for prototype n°1. A better efficiency for the WPTS is therefore achieved with the LW n°2 although its copper surface is 2.5 times smaller than that of the LW n°1. Characteristics of the two LW are compared in Table 3.

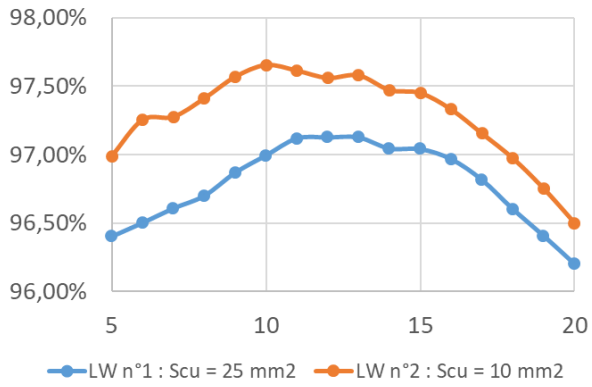

Fig 12: Efficiency DC to DC of the WPTS n°1 (Blue) and n°2 (Orange) as a function of output power in kW.

	LW n°1	LW n°2
Copper section	25 mm2	10 mm2
Current density 1R	1.35 A/mm2	3.37 A/mm2
Current density 2R	1.87 A/mm2	4.67 A/mm2
Weight per meter	223 g/m	89 g/m
Price per meter	21.4 €/m	6.3 €/m
Total price	788 €	232 €
WPTS efficiency	96.2 %	96.5 %

Table 3: LW comparison on physical and economical aspects.

Prototype n°2 allowed a 20% reduction in winding losses while dividing their cost by a factor of 3.4. This price reduction is achieved by the less complex design of LW n°2 and by reducing the copper surface by a factor of 2.5.

4 Outlook

The study and experiments in this article have shown the performance and cost savings that can be achieved by designing LW according to the recommendations. Design limitations due to high frequencies and currents in excess of hundreds of amperes may occur. However, Table ***3*** shows the strong interest in respecting the design rules. The LW n°2 shows indeed a current density 2.5 times higher and a better efficiency at the same time than the LW n°1.

In addition, the rising price of copper from 1,897 €/t to 6,564 €/t between February 2000 and January 2021 shows the growing economic interest in minimising the copper surface.

5 Conclusion

This article presents new comparisons of Litz wires subjected to a root mean square current of 30 A. Tests are also carried out on two WPTS with an output power of 20 kW. The considerable impact of bundles number per level on current distribution was measured, showing several bundles current in phase opposition with the LW current. The influence of LW design over current distribution is dominant ahead of the connectors and the external field as shown in the tests parts 3.2 and 3.3.

A good design respecting the following rules will limit bundles skin and proximity effects. For this purpose, five bundles maximum per level is required, except on the first level where the sub-bundles are made of strands. The maximum strands number per bundles is indicated in [17].

The new WPTS prototype made with LW n°2 according to the recommendations allows:

- A cost saving of a factor of 3.4
- A 20% reduction in winding losses
- A reduction in the quantity of Copper by a factor 2.5

6 References:

[1] M. Zamani, M. Nagrial, J. Rizk, et A. Hellany, « A review of inductive power transfer for electric vehicles », in *2019 International Conference on Electrical Engineering Research Practice (ICEERP)*, nov. 2019, p. 1-5, doi: 10.1109/ICEERP49088.2019.8956971.

[2] W. Wenbin *et al.*, « A Review of High Power Research on Electric Vehicle Wireless Charging », in *2019 14th IEEE Conference on Industrial Electronics and Applications (ICIEA)*, juin 2019, p. 2552-2557, doi: 10.1109/ICIEA.2019.8833765.

[3] V. Shevchenko, O. Husev, R. Strzelecki, B. Pakhaliuk, N. Poliakov, et N. Strzelecka, « Compensation Topologies in IPT Systems: Standards, Requirements, Classification, Analysis, Comparison and Application », *IEEE Access*, vol. 7, p. 120559-120580, 2019, doi: 10.1109/ACCESS.2019.2937891.

[4] K. Aditya et S. S. Williamson, « Comparative study of series-series and series-parallel topology for long track EV charging application », in *2014 IEEE Transportation Electrification Conference and Expo (ITEC)*, juin 2014, p. 1-5, doi: 10.1109/ITEC.2014.6861793.

[5] Y. Chen, H. Zhang, C.-S. Shin, K.-H. Seo, S.-J. Park, et D.-H. Kim, « A Comparative Study of S-S and LCC-S Compensation Topology of Inductive Power Transfer Systems for EV Chargers », in *2019 IEEE 10th International Symposium on Power Electronics for Distributed Generation Systems (PEDG)*, juin 2019, p. 99-104, doi: 10.1109/PEDG.2019.8807684.

[6] Y. Wanderoild, A. Morel, R. Grezaud, G. Pillonnet, D. Bergogne, et H. Razik, « Optimal Compensation Capacitors Maximizing Coreless Inductive Power Transfer », in *PCIM Europe 2017; International Exhibition and Conference for Power Electronics, Intelligent Motion, Renewable Energy and Energy Management*, mai 2017, p. 1-7.

[7] J. Sallan, J. L. Villa, A. Llombart, et J. F. Sanz, « Optimal Design of ICPT Systems Applied to Electric Vehicle Battery Charge », *IEEE Transactions on Industrial Electronics*, vol. 56, nº 6, p. 2140-2149, juin 2009, doi: 10.1109/TIE.2009.2015359.

[8] Y. Tono, H. Omori, T. Iwanaga, H. Michikoshi, et K. Sakamoto, « A High-Power Miniaturized Wireless EV Charger with a New SiC-VMOSFET driven Single-Ended Inverter », in *PCIM Asia 2019; International Exhibition and Conference for Power Electronics, Intelligent Motion, Renewable Energy and Energy Management*, juin 2019, p. 1-8.

[9] C. Wei, D. Zhu, H. Xie, et J. Shao, « A 6.6kW high power density bi-directional EV on-board charger based on SiC MOSFETs », in *PCIM Europe 2019; International Exhibition and Conference for Power Electronics, Intelligent Motion, Renewable Energy and Energy Management*, mai 2019, p. 246-252.

[10] C. Wei, D. Zhu, H. Xie, Y. Liu, et J. Shao, « A SiC-Based 22kW Bi-directional CLLC Resonant Converter with Flexible Voltage Gain Control Scheme for EV On-Board Charger », in *PCIM Europe digital days 2020; International Exhibition and Conference for Power Electronics, Intelligent Motion, Renewable Energy and Energy Management*, juill. 2020, p. 1-7.

[11] R. Bosshard, J. W. Kolar, J. Mühlethaler, I. Stevanović, B. Wunsch, et F. Canales, « Modeling and $\eta $ - $\alpha $ -Pareto Optimization of Inductive Power Transfer Coils for Electric Vehicles », *IEEE Journal of Emerging and Selected Topics in Power Electronics*, vol. 3, nº 1, p. 50-64, mars 2015, doi: 10.1109/JESTPE.2014.2311302.

[12] O. C. Onar, S. L. Campbell, L. E. Seiber, C. P. White, et M. Chinthavali, « A high-power wireless charging system development and integration for a Toyota RAV4 electric vehicle », in *2016 IEEE Transportation Electrification Conference and Expo (ITEC)*, juin 2016, p. 1-8, doi: 10.1109/ITEC.2016.7520247.

[13] O. C. Onar, M. Chinthavali, S. L. Campbell, L. E. Seiber, C. P. White, et V. P. Galigekere, « Modeling, Simulation, and Experimental Verification of a 20-kW Series-Series Wireless Power Transfer System for a Toyota RAV4 Electric Vehicle », in *2018 IEEE Transportation Electrification Conference and Expo (ITEC)*, juin 2018, p. 874-880, doi: 10.1109/ITEC.2018.8450085.

[14] B. SARRAZIN, A. DERBEY, P. ALBOUY, J.-P. FERRIEUX, G. MEUNIER, et J.-L. SCHANEN, « Bidirectional Wireless Power Transfer System with Wireless Control for Electrical Vehicle », in *2019 IEEE Applied Power Electronics Conference and Exposition (APEC)*, mars 2019, p. 3137-3143, doi: 10.1109/APEC.2019.8721800.

[15] C. Ziegler, S. Weber, G. Heiland, et D. Kraus, « Influences of WPT-Coil Losses and Coupling Coefficient on the Resonance Circuits of Wireless Power Transfer Systems », in *PCIM Europe 2017; International Exhibition and Conference for Power Electronics, Intelligent Motion, Renewable Energy and Energy Management*, mai 2017, p. 1-7.

[16] S. Gyimóthy *et al.*, « Loss Computation Method for Litz Cables With Emphasis on Bundle-Level Skin Effect », *IEEE Transactions on Magnetics*, vol. 55, nº 6, p. 1-4, juin 2019, doi: 10.1109/TMAG.2019.2890969.

[17] C. R. Sullivan et R. Y. Zhang, « Simplified design method for litz wire », in *2014 IEEE Applied Power Electronics Conference and Exposition - APEC 2014*, mars 2014, p. 2667-2674, doi: 10.1109/APEC.2014.6803681.

[18] T. B. Gradinger et U. Drofenik, « Managing high currents in litz-wire-based medium-frequency transformers », in *2018 20th European Conference on Power Electronics and Applications (EPE'18 ECCE Europe)*, sept. 2018, p. P.1-P.10.

[19] D. Barth, T. Leibfried, et G. Cortese, « Analytical calculation of the frequency-dependent litz wire resistance considering the wire connectors », in *2019 21st European Conference on Power Electronics and Applications (EPE '19 ECCE Europe)*, sept. 2019, p. P.1-P.10, doi: 10.23919/EPE.2019.8915419.

[20] A. Roßkopf, E. Bär, et C. Joffe, « Influence of Inner Skin- and Proximity Effects on Conduction in Litz Wires », *IEEE Transactions on Power Electronics*, vol. 29, nº 10, p. 5454-5461, oct. 2014, doi: 10.1109/TPEL.2013.2293847.

[21] Le Guipage Moderne, « NOTE D'APPLICATION POUR L'ETAMAGE DES FILS DE LITZ EN CUIVRE EMAILLE SOUDABLE GRADE 1 OU 2 TEMPERATURE 155°C OU 180 °C ». févr. 01, 2021, [En ligne]. Disponible sur: https://leguipagemoderne.pagesperso-orange.fr/pages/catalogue.htm.

[22] New England Wire, « Litz Wire Termination Guide ». févr. 01, 2021, [En ligne]. Disponible sur: https://www.newenglandwire.com/litz-wire-termination-guide/.

[23] J. Acero, P. J. Hernandez, J. M. Burdio, R. Alonso, et L. A. Barragdan, « Simple resistance calculation in litz-wire planar windings for induction cooking appliances », *IEEE Transactions on Magnetics*, vol. 41, nº 4, p. 1280-1288, avr. 2005, doi: 10.1109/TMAG.2005.844844.

[24] J. Acero, R. Alonso, J. M. Burdio, L. A. Barragan, et D. Puyal, « Frequency-dependent resistance in Litz-wire planar windings for domestic induction heating appliances », *IEEE Transactions on Power Electronics*, vol. 21, nº 4, p. 856-866, juill. 2006, doi: 10.1109/TPEL.2006.876894.

[25] R. Tanzania, F. H. Choo, et L. Siek, « Design of WPT coils to minimize AC resistance and capacitor stress applied to SS-topology », in *IECON 2015 - 41st Annual Conference of the IEEE Industrial Electronics Society*, nov. 2015, p. 000118-000122, doi: 10.1109/IECON.2015.7392085.

[26] Z. Luo et X. Wei, « Analysis of Square and Circular Planar Spiral Coils in Wireless Power Transfer System for Electric Vehicles », *IEEE Transactions on Industrial Electronics*, vol. 65, nº 1, p. 331-341, janv. 2018, doi: 10.1109/TIE.2017.2723867.

[27] V. Väisänen, J. Hiltunen, J. Nerg, et P. Silventoinen, « AC resistance calculation methods and practical design considerations when using litz wire », in *IECON 2013 - 39th Annual Conference of the IEEE Industrial Electronics Society*, nov. 2013, p. 368-375, doi: 10.1109/IECON.2013.6699164.